Paper ID: 409

Green Synthesis of Magnetite Nanoparticles and Study of Its Morphological, Structural, and Magnetic Properties

Mashuk Jahir[1], Sneha Das Puza[2], Umme Salma Mst. Mahmuda[3]
[1,2,3] Department of Materials Science & Engineering, Rajshahi University of Engineering & Technology. Rajshahi-6204
E-mail: mashukjahir.j@gmail.com, snehapuja1309@gmail.com, mahmuda@mse.ruet.ac.bd

Abstract

In the age of nanotechnology, magnetite (Fe_3O_4) nanoparticles (NPs) play a huge role. These nanoparticles may be used in a number of biomedical fields, including magnetic hyperthermia, targeted medication delivery, bacterial killing, and magnetic resonance imaging. In this study, Cinnamomum camphora leaf extract, which serves as an effective stabilizer and capping agent for the nanoparticles, was used to create Fe_3O_4 NPs by an economical and environmentally friendly "Green Synthesis" method. The X-ray Diffraction (XRD) investigation revealed that the particles were crystalline with cubic inverse spinel structure and the crystallite size was determined to be approximately 15.6 ± 0.8 nm. Scanning electron microscopy (SEM) was used to examine the surface morphology of the NPs, and the result indicated that the NPs had a uniform size distribution and spherical in shape. Energy Dispersive X-ray (EDX) Spectroscopy was used to analyze the NPs' elements, and the result showed that iron and oxygen were present in the nanoparticles. The functional groups alcohol, alkene, and alkyne were present in the capping agents of the nanoparticles, according to the Fourier Transform Infrared Spectroscopy (FTIR) analysis. Using a vibrating sample magnetometer (VSM), it was determined that the NPs were superparamagnetic in nature and had very low coercivity and remnant magnetization.

Keywords: Magnetite, green synthesis, superparamagnetic, nanoparticles, magnetization.

1. Introduction

Nanotechnology created nanoparticles with special physical, chemical, and magnetic capabilities, it transformed many scientific domains, including biomedical applications. Among these, magnetite (Fe_3O_4) nanoparticles have drawn a lot of attention because of their low toxicity, huge surface area, superparamagnetic qualities, and biocompatibility [1]. Conventional techniques for creating these nanoparticles frequently call for the employment of dangerous chemicals, high pressures, and temperatures. Green synthesis techniques that make use of plant extracts have consequently become a sustainable substitute [2]. The green synthesis of Fe_3O_4 nanoparticles utilizing *Cinnamomum camphora* leaf extract is the main focus of this paper. The leaf extract facilitates the creation of nanoparticles with regulated morphology and stability by acting as a reducing and capping agent. The structural, morphological, and magnetic characteristics of the produced nanoparticles were subsequently investigated utilizing a variety of analytical methods.

2. Materials and Methodology

2.1.Materials

The primary iron sources utilized were ferric chloride anhydrous ($FeCl_3$) and ferrous chloride tetrahydrate ($FeCl_2 \cdot 4H_2O$). Sodium hydroxide (NaOH) served as the base. Natural reducing agent was derived from extracts of *Cinnamomum camphora* leaves. All chemicals were of analytical grade and were used without any additional purification. De-ionized water (DI water) was employed for the preparation of all solutions.

2.2.Leaf Extracts Preparation

Cinnamomum camphora leaf extract was made by gathering healthy leaves from nearby sources, washing them to get rid of dust, and then letting them air dry for a whole day in an environment free of dust. To make a fine

paste, the dried leaves were chopped, ground into and sieved. After that, 200 mL of de-ionized water was combined with 15 g of the paste, and the mixture was heated to 80 °C for 4 hours and 30 minutes. The combination was filtered after two hours to extract the leaf extract, which was then kept for further experiments at 4 °C.

2.3.Synthesis of Fe_3O_4 Nanoparticles

For the synthesis of Fe_3O_4 nanoparticles first 30 mL of the 0.25 M $FeCl_2 \cdot 4H_2O$ solution and 30 mL of the 0.5 M $FeCl_3$ solution were mixed in a separate beaker with a magnetic stirrer . After 20 minutes of stirring, 6 mL of *Cinnamomum camphora* leaf extract was added, and stirring continued. Following another 20 minutes, 150 mL of 0.5 M NaOH solution was added, turning the solution black, indicating the formation of Fe_3O_4 NPs. The NPs were separated using a magnetic separator, dried in an oven at 60 °C, and stored at 4 °C for further characterization. Fe_3O_4 NPs were synthesized via a facile green synthesis route where $FeCl_3$ and $FeCl_2$.4H2O were used as precursor and *Cinnamomum camphora* leaf extract was used as a source of reducing and capping agents. To synthesis Fe_3O_4 the *Cinnamomum camphora* leaf extract added to an aqueous mixture of Fe^{3+} and Fe^{2+} chloride at a 2:1M ratio. The chemical reaction of Fe_3O_4 precipitation is given below. The overall reaction may be written as follows:

Cinnamomum camphora + H_2O (l) +Fe^{2+}(aq) + Fe^{3+}(aq) ⟶

[*Cinnamomum camphora* /Fe^{3+}-Fe^{2+}] …….... (2.1)

[*Cinnamomum camphora* /Fe^{3+}-Fe^{2+}] + $8OH^-_{(aq)}$ ⟶

[*Cinnamomum camphora* /Fe_3O_4] $\downarrow_{(s)}$ + $4H_2O_{(aq)}$ … (2.2)

3. Results and Discussion

3.1 XRD pattern analysis of Fe_3O_4 NPs

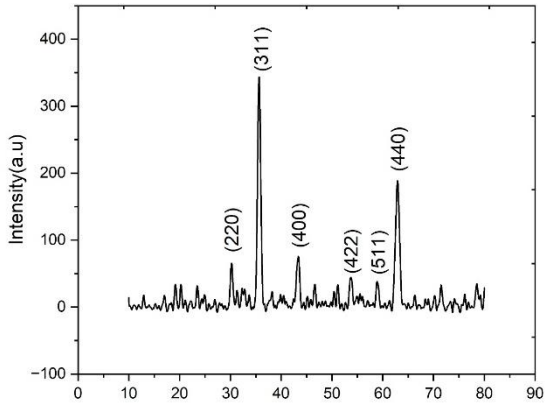


Figure 1: XRD pattern of Fe3O4 NPs

Fe_3O_4 NPs were characterized by XRD for structural determination and estimation of crystallite size. All the peaks of XRD patterns were analyzed and indexed after comparing with magnetite (Fe_3O_4) standards (JCPDS card no. 01-075- 0033) [3]. The peaks indexed at 2θ = 30.24, 35.66, 43.32, 53.74, 58.95, 62.91 as planes (220), (311), (400), (422), (511) and (440) are corresponded to a cubic unit cell, characteristic of a cubic inverse spinal structure shown in Fig. 1[4]

The distinct brightest reflection that emerged from the (311) plane provided more evidence for the cubic inverse spinal structure. Fe_3O_4 diffraction peaks were the only ones visible, suggesting that extremely phase-pure Fe3O4 particles were produced. Crystallite size measurements were made using the Scherrer approximation, which postulates that small crystallite size is the cause of line broadening, and the full-width at half maximum (FWHM) of the greatest reflection of the (311) peak [5].

$D = K\lambda / \beta cos\theta$ …… 3.1

Here, D is the crystallite size; k is the shape parameter, which is 0.89 for magnetite, λ is the X-ray wavelength (0.15406 nm), β the full width at half maximum (FWHM) in radians in the 2θ scale, and θ is the Bragg angle. Taking the highest intensity peak, namely the (311) plane, at 2θ = 35.66 for which FWHM is 0.69893, the crystal size calculated were 11.94 ± 0.8 nm.

From this XRD analysis the structural parameter such as dislocation density, macrostrain are also determined. The dislocation density is a measure of the number of dislocations in a unit volume of a crystalline material. Macrostrain refers to the overall change in the lattice parameters caused by a composition change or temperature change or pressure change [6]. The dislocation density and macrostrain of Fe_3O_4 NPs were calculated by using following formula, respectively.

$\delta = 1/ D^2$ …….. (3.2)

$\varepsilon = \beta cos\theta/4$ …….. (3.3)

where, D is the crystallite size which is calculated using Scherrer approximation and β is the FWHM which is obtained from XRD analysis of Fe_3O_4 NPs. The structural parameter of Fe_3O_4 NPs obtained from XRD analysis are shown in table 1.

Table 1:Structural parameters of Fe3O4 NPs obtained from XRD analysis

Plane (hkl)	FWHM (deg)	Crystallite sizeD (nm)	Dislocation density (δ) Line/nm^2 × 10^{-3}	Macrostrain (ε) × 10^{-3}
(200)	0.51	16.03	3.89	8.28
(311)	0.69	11.94	7.01	9.47
(400)	0.66	12.90	6.00	7.27
(422)	0.57	15.55	4.13	4.93
(511)	0.50	17.98	3.09	3.91
(440)	0.87	10.64	8.81	6.23

3.2 FT-IR analysis of Fe_3O_4 NPs

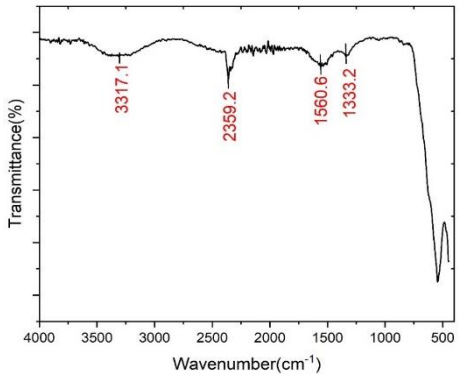


Figure 2: FT-IR spectrum of Fe_3O_4 NPs

FT-IR spectroscopy was performed to determine the functional groups of leaf extract those acted as a stabilizer and capping agent in the synthesized of Fe_3O_4 NPs. The spectra of the Fe_3O_4 NPs synthesized with leaf extract revealed absorption bands at 3317, 2359.2, 1560, and 1333 cm-1 as shown in Fig. 2. The peak at 3317.1 cm-1 corresponds to the –OH stretching frequency, 2359.2 cm-1 corresponds to the C≡N stretching vibrations, 1560.6 cm−1 for conjugated carbonyl (–C=O) group stretching vibrations.[7]

3.3 SEM analysis

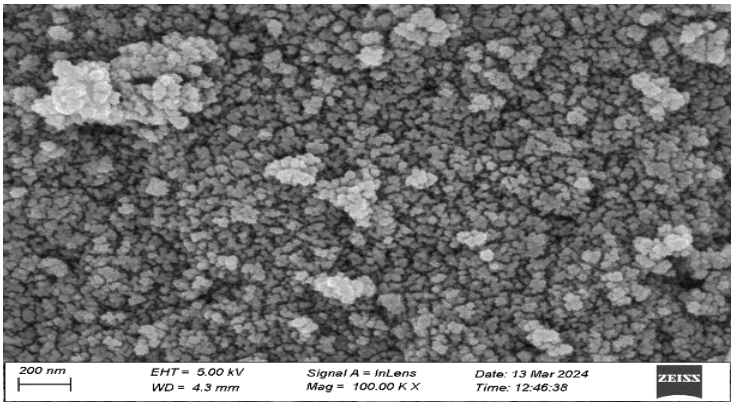


Figure.3: SEM image of surface morphology of Fe_3O_4 NPs

SEM was used to examine the surface morphology and homogeneity of the manufactured Fe_3O_4 NPs, as seen in Fig. 3. The SEM picture demonstrates the crystallinity of the Fe_3O_4NPs, whose uniform surface morphology is observed to be spherical in form. The greatest amount of charges on the surface of NPs increases the surface energy. Consequently, the spherical shape of NPs was caused by a particle's stronger surface tension than larger particles. The produced Fe_3O_4 NPs' SEM picture shows that the particles are evenly scattered throughout the nanometer range.

3.3.1 Particle size distribution Fe_3O_4 NPs

From the histogram we can see that most of the particles are sized between 25-30 nm. The average size of particles calculated from the histogram is 27.13 nm.

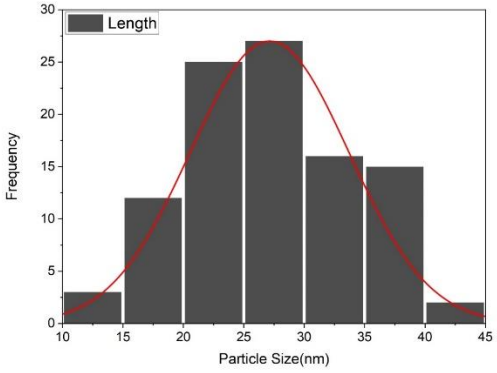


Figure 4: Size distribution of Fe_3O_4 NPs

3.4 EDX spectrum analysis

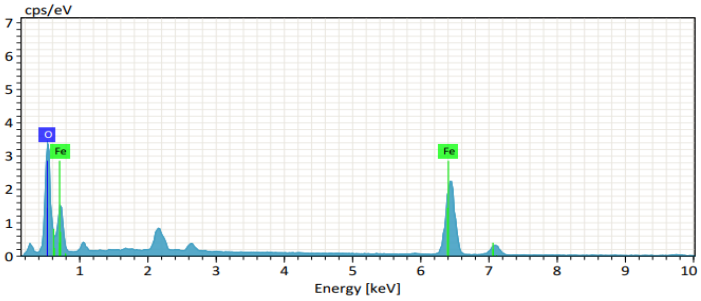


Figure 5: EDX spectrum of Fe_3O_4 NPs

A study of the elemental components of the produced Fe_3O_4 NPs was done using EDX spectroscopy. The elemental signature of the existence of oxygen (O) and iron (Fe) is indicated by the EDX spectra seen in Figure 5. The EDS spectra show two strong peaks at around 0.5 keV and 6.4 keV, respectively, showing the presence of O and Fe, which contribute to the binding energy of iron and oxygen, respectively, and correlate to the Fe_3O_4 NPs. A less strong peak of Fe at.7 keV is associated with the Fe_3O_4 NPs' surface. The presence of the Fe_3O_4 NPs' constituent elements is confirmed by this result [8][9].

3.5 Magnetization analysis

The magnetic property of room-temperature produced Fe_3O_4 NPs was examined using VSM. The produced NPs' saturation magnetization was found to be approximately 15.7 emu/g, which is less than its bulk value of 92 emu/g [10]. The canted or disordered spins on the NPs' surface are thought to be preventing the core spins from aligning along the direction of the field, which lowers the saturation magnetization of the tiny NPs [11]. A notable decrease in magnetization value is obtained as a result of increased surface pain canting resulting from a greater decrease in particle size [12]. It is clear from the curve (Fig. 6) that there is a very narrow hysteresis loop with a remnant magnetization value of .34 emu/g and coercivity of 43.74 Oe. Superparamagnetism typically occurs in materials with very small crystallites, i.e. less than 30 nm.[13] The narrow hysteresis loop, low remnant magnetization, and low coercivity are indicative of superparamagnetic behavior because superparamagnetic particles do not retain any magnetization in the absence of an external magnetic field. This is due to the thermal energy being sufficient to randomly flip the magnetic moments of the particles, resulting in zero net magnetization. When an external magnetic field is applied, the magnetic moments align with the field, but once the field is removed, the thermal agitation causes the moments to randomize again, leading to low remnant magnetization and coercivity.[14][15][16]

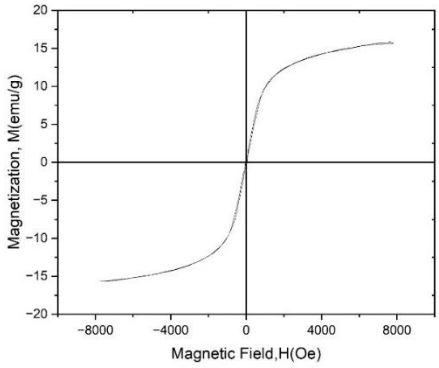


Figure 6: Magnetization curve of *Fe_3O_4* NPs synthesized with .5M NaOH

Conclusion

This study used $FeCl_2$ and $FeCl_3$ as precursors and *Cinnamomum camphora* leaf extract as a source of reducing, capping, and stabilizing agents. As a result, Fe_3O_4 NPs with the inverse spinel cubic crystalline structure were produced efficiently. The formation, stability, and bioreduction of Fe_3O_4 NPs may be influenced by a variety of biomolecules included in leaf extract, such as polysaccharides, alcoholic compounds, proteins/enzymes, vitamins, and alkaloids. The ion reduction potential and reducing capacity of leaf extract have a major influence on the production of NPs. On the basis of the XRD pattern, the average crystallite size of the produced inverse spinel cubic crystalline types Fe_3O_4 NPs was calculated to be 15.6 ± 0.8 nm. EDX spectra verified the presence of the elemental components of the Fe_3O_4 NPs. FT-IR spectroscopy showed that biomolecules present in *Cinnamomum camphora* extract were involved, and the production of Fe_3O_4 NPs validated this involvement. Because of the capping agents that stabilize the Fe_3O_4 NPs, the surface morphology was found to be homogenous and nearly spherical in form with low agglomeration, as shown by the SEM image, which also showed the crystallinity of the generated Fe_3O_4 NPs. According to the VSM analysis of the generated Fe_3O_4 NPs' magnetic properties, the synthesized Fe_3O_4 NPs exhibited superparamagnetic characteristics with extremely low corrosivity and remanence magnetization properties.

References

[1] Jiri, K., Yazan, H., Lukas, R., Zbynek, H., Mirko, C., Vojtech, A., Ondrej, Z., "Magnetic nanoparticles: From design and synthesis to real world applications," J. Nanomater, vol. 7, pp. 243-273, 2017.

[2] Pratyusha, B., Debjani, N., "Plants and eco-friendly nanomaterials- A review," Conference Paper, pp. ISBN 978, 2015.

[3] Ausloos, P., Clifton, C. L., Lias, S. G., Mikaya, A. I., Stein, S. E., Tchekhovskoi, D. V., "The critical evaluation of a comprehensive mass spectral library," J. Am. Soc. Mass Spectrom, vol. 10, p. 287–299, 1998.

[4] Vaidyanathan G, Sendhilnathan S, Arulmurugan R. Structural and magnetic properties of Co1-xZnxFe2O4 nanoparticles by coprecipitation method. J Magn Mater. 2007;313:293.

[5] Marlene, C. M., Howard, F. M., Eloise, H. E., "Standard x-ray diffraction powderpatterns," J. Res. Natl. Bur. Stand., vol. 18, pp. 36-40, 1981.

[6] Davor, B., "X-ray diffraction line broadening: modeling and applications to high-tc superconductors," J. Res. Natl. Inst. Stand. Technol., vol. 98, p. 321–353, 1993.

[7] Amutha, S., & Sridhar, S. (2018). Green synthesis of magnetic iron oxide nanoparticle using leaves of Glycosmis mauritiana and their antibacterial activity against human pathogens. Journal of Innovations in Pharmaceutical and Biological Sciences, 5(2), 22-26.

[8] Sen, S. K., Barman, U. C., Manir, M. S., Mondal, P., Dutta, S., Paul, M., Chowdhury, M. a. M., & Hakim, M. A. (2020). X-ray peak profile analysis of pure and Dy-doped α-MoO3 nanobelts using Debye-Scherrer, Williamson-Hall and Halder-Wagner methods. Advances in Natural Sciences Nanoscience and Nanotechnology, 11(2), 025004.

[9] William, H. C.,Martin J. C., Robert, A. G., "Crystal defects and the dissolution kinetics of rutile," Geochim. Cosmochim. Acta, vol. 52, pp. 1545-1556, 1988.

[10] Nicolae, C. P., Davor, B., Sven, C. V., "Elastic macro strain and stress determination by powder diffraction: spherical harmonics analysis starting from the Voigt model," J. Appl. Cryst., vol. 47, p. 154 –159, 2014.

[11] Sole, V.A., Papillon, E., Cotte, M., Walter, P., Susini, J., "A multiplatform code for the analysis of energy-dispersive X-ray fluorescence spectra," Spectrochim. Acta, Part B, vol. 62, p. 63–68, 2007.

[12] Di, Z., Amar B. K., Dan, R., David, P. Y., Andrew, W., David, C., Thomas, H. H., Zhanhu, G., "Electrospun polyacrylonitrile nanocomposite fibers reinforced with Fe3O4 nanoparticles: Fabrication and property analysis," Polym. J., vol. 50, p. 4189–4198, 2009.

[13] Palanisamy, K. Lakshmanan, Kesavan Vignesh, and Nanjappan Karthikeyan. "Applications and Toxicology of Iron Oxide Nanoparticles." Iron Ores and Iron Oxides-New Perspectives. IntechOpen, 2023.

[14] Cregg, P., Murphy, K., & Mardinoglu, A. (2011). Inclusion of interactions in mathematical modelling of implant assisted magnetic drug targeting. Applied Mathematical Modelling, 36(1), 1–34.

[15] Andersson, R. L., et al. "Superparamagnetic [sic] nanofibers by electrospinning." RSC advances 6.26 (2016): 21413-21422.

[16] Kershi, R. M., F. M. Ali, and M. A. Sayed. "Influence of rare earth ion substitutions on the structural, optical, transport, dielectric, and magnetic properties of superparamagnetic iron oxide nanoparticles." Journal of Advanced Ceramics 7 (2018): 218-228.